

# Chapter 15

## The SuperCDMS Experimental Program

Enectali Figueroa-Feliciano

**Abstract** The Super Cryogenic Dark Matter Search (SuperCDMS) experimental program is underway. The Soudan experiment is currently taking data with a 10 kg detector payload, and a generation 2 experiment at SNOLAB with a 200 kg payload has been proposed. First results from the SuperCDMS Soudan experiment are expected in 2013. The Soudan and SNOLAB experiments will reach a sensitivity to the WIMP-nucleon cross section of  $5 \times 10^{-45} \text{ cm}^2$  and  $8 \times 10^{-47} \text{ cm}^2$ , respectively, for WIMP masses around  $60 \text{ GeV}/c^2$ . Using new low-threshold techniques, both experiments are expected to achieve world-leading sensitivities to WIMP masses between 2 and  $10 \text{ GeV}/c^2$ . In this paper we give an overview of the SuperCDMS experimental program and report on the discrimination capability of our new iZIP detectors.

### 15.1 SuperCDMS Overview

Measurements from the cosmic microwave background, supernovae, and large scale structure, among others, are fit by a simple six-parameter concordance model of cosmology [1]. This model requires cold dark matter, a non-baryonic form of matter that accounts for 82 % of the matter content of the Universe. One of the favored candidates for this form of matter is the Weakly Interacting Massive Particle (WIMP), which arises naturally in many theories for physics beyond the standard model.

A worldwide experimental search for potential interactions between cosmological dark matter particles and underground detectors is ongoing. The Super Cryogenic Dark Matter Search (SuperCDMS) experiment uses arrays of germanium crystal detectors operated at millikelvin temperatures to search for these rare interactions.

---

E. Figueroa-Feliciano (✉)  
Massachusetts Institute of Technology, Cambridge, MA 02139, USA  
SuperCDMS Collaboration  
e-mail: enectali@mit.edu; [http://cdms.berkeley.edu/cdms\\_collab.html](http://cdms.berkeley.edu/cdms_collab.html)

Discrimination between signals and backgrounds is done through the measurement of both the ionization and thermal phonon signals produced by each event in a crystal. These two signals are measured by multiple ionization electrodes and phonon sensors on the top and bottom faces of the crystal. The timing, pulse shapes, and relative amplitudes of these high signal-to-noise measurements encode a wealth of information about each event. Since the ratio between the ionization and phonon signals (called the yield) is different for electron and nuclear recoils, these measurements allow excellent event-by-event discrimination between these two type of interactions. The modular design allows for accurate measurement of the background rejection capability and the background levels at the individual crystal and sub-assembly levels, allowing accurate predictions of the sensitivity of future experiments well before the experiment is under operation.

The SuperCDMS Soudan experiment is currently operating an array of 15 Ge detectors with a total mass of 10 kg at the Soudan mine in Minnesota. We expect the first results from this experiment in 2013. Both a “standard” near-zero-background analysis with maximum sensitivity for WIMPs of around 60 GeV/c<sup>2</sup> and a “lowthreshold” analysis with non-zero background optimized for the sub-10 GeV/c<sup>2</sup> mass region will be performed. The expected sensitivity of both analyses are shown in Fig. 15.1.

SuperCDMS Soudan is the first experiment to use our new iZIP detector technology. These detectors have a new sensor layout which provides excellent discrimination sufficient for a near-zero background experiment with a mass of several hundred kilograms. To exploit this capability, a new experiment is needed.

SuperCDMS SNOLAB is a proposed 200 kg payload of 100 mm diameter, 1.4 kg mass germanium detectors in a new lower-background set up with a sensitivity of  $8 \times 10^{-47} \text{ cm}^2$  to 60 GeV/c<sup>2</sup> WIMPs. The experiment would follow the successful CDMS philosophy of building up the mass through a set of towers of 6 detectors each, which can be individually tested at test facilities. A set of 24 towers arranged in a low-background cryogenic copper shield (the “SNObox”) would form the core of the experiment, surrounded by a set of external room-temperature shields made of polyethylene or water and lead. An active neutron veto detector is also being considered. Two penetrations would be used for to connect the cryogenic stages to a dilution refrigerator and to route the electronics wiring. A pre-conceptual design is shown in Fig. 15.2.

## 15.2 SuperCDMS Detectors

A schematic of the new interleaved Z-sensitive Ionization and Phonon (iZIP) detectors used for SuperCDMS Soudan is shown in Fig. 15.3. Phonon and ionization sensors are lithographically deposited on the top and bottom surfaces of a high-purity 76 mm diameter by 25 mm thick germanium crystal. The sensors meander around the surface, forming an interleaved pattern with four individual phonon sensors (three in the center, one forming a ring at the perimeter) and two charge channels (an inner channel and a thin outer ring at the perimeter). The thick lines in

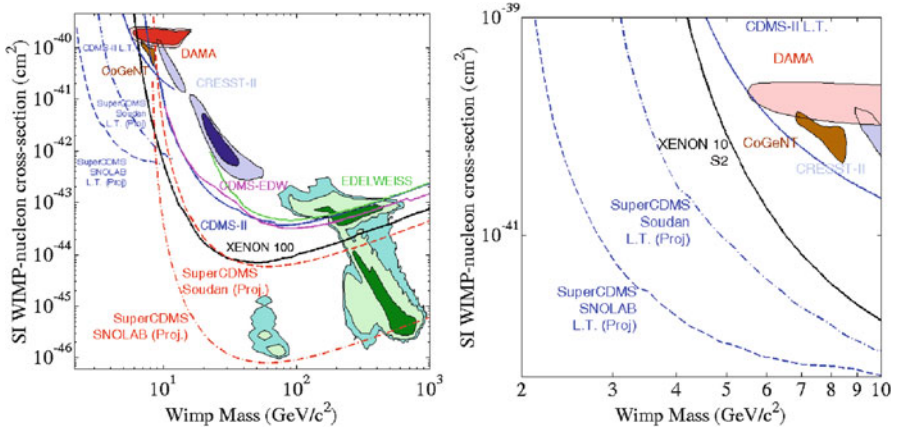


**Fig. 15.1** *Left:* Recent upper limits (90 % C.L.) on the WIMP-nucleon spin-independent cross section versus WIMP mass are shown from *top to bottom* for CDMS II Soudan [2, 3] (*blue solid*), EDELWEISS II [4] (*green solid*), combined CDMS-EDELWEISS II [5] (*magenta*), and XENON100 [6] (*black solid*). The *blue filled* region indicates the region where CRESST II reports a signal [7]: 1-sigma allowed region (*dark blue*), 2 sigma allowed region (*light blue*). The *red dotted* portions of the graph indicate the regions where DAMA reports a signal [8]: 90 % C.L. (*red*), and 99 % C.L. (*dark red*). The *colored* regions show the current cMSSM regions (with recent LHC and Higgs constraints) predicting where WIMPs may be found, assuming flat priors: Stregé et al. [9], at 68 % (*green*), 95 % (*light green*), and 99 % (*cyan*) C.L. Also shown are projected sensitivities for the SuperCDMS Soudan experiment (*dashed red*) and the proposed SuperCDMS SNOLAB experiment with a 200 kg payload for 4 years running (*dot-dashed red*); these assume no background subtraction. Finally, low-threshold SuperCDMS Soudan (*dot-dashed blue*) and SuperCDMS SNOLAB (*dashed blue*) projections are also shown. *Right:* Same figure, except zoomed-in on the low WIMP mass region, highlighting the reach of SuperCDMS with its low energy thresholds (Color figure online)

the schematic are the phonon meanders, while the charge lines are very thin and are barely visible in the figure.

The phonon sensors on both sides of the crystal are operated at a potential of 0 V, while the charge channels are biased at +2 V on the top surface and -2 V at the bottom. This creates a fairly homogeneous vertical field in the bulk of the crystal, while the top and bottom surfaces have a complex field structure as shown in Fig. 15.3 (right). When events occur near the surface of the crystal, they experience a field that is predominantly in the transverse direction. The electrons and holes created follow this field and are sensed only by the electrodes on that surface. Events happening in the bulk see a vertical field and thus ionization signals are produced both on the bottom and top ionization channels. A measured asymmetry in the charge signals between the top and the bottom sensors thus indicates the event is a surface event. Phonon sensors on both sides measure the total energy and contain a trove of information in their pulse shapes and timing which we are only beginning to study but which already shows discrimination potential between surface and bulk events and also between electron and nuclear recoils.

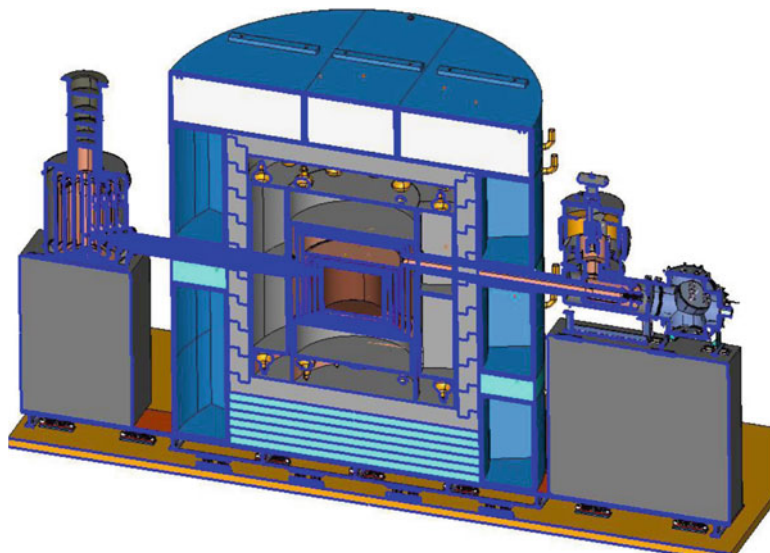


**Fig. 15.2** Pre-conceptual design of the new SuperCDMS facility at SNOLAB. The dilution refrigerator on the *left side* of the diagram provides the cooling for the thermal layers surrounding the detectors (*center*). An additional cooling unit and electronics breakout box are to the *right*. The neutron veto detector under consideration would be inside the Pb shielding, which is surrounded by a massive polyethylene (or water) shield

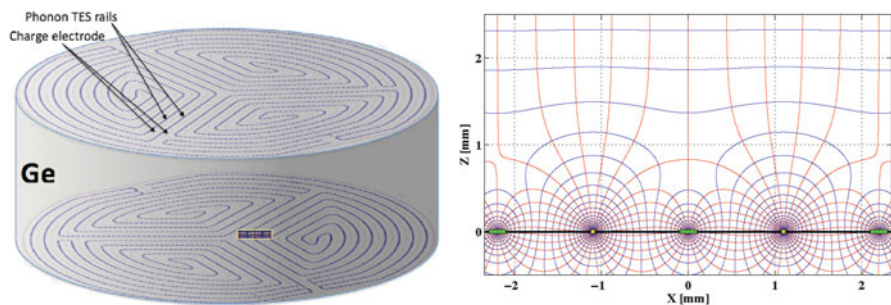


**Fig. 15.3** *Left*: Phonon and ionization sensor layout for iZIP detector deployed at Soudan. The two faces are instrumented with interleaved ionization and phonon sensors. The phonon sensors are arranged to give 4 phonon readout channels for each face, an outer sensor surrounding three inner ones. The small yellow rectangle is the approximate location of the cross section shown on the *right*. *Right*: Magnified cross section view of electric field lines (*red*) and equipotential contours (*blue*) near the bottom face of a SuperCDMS iZIP detector. The ionization electrode lines (*yellow squares*) are narrower than the athermal phonon collection sensors (*green rectangles*) (Color figure online)

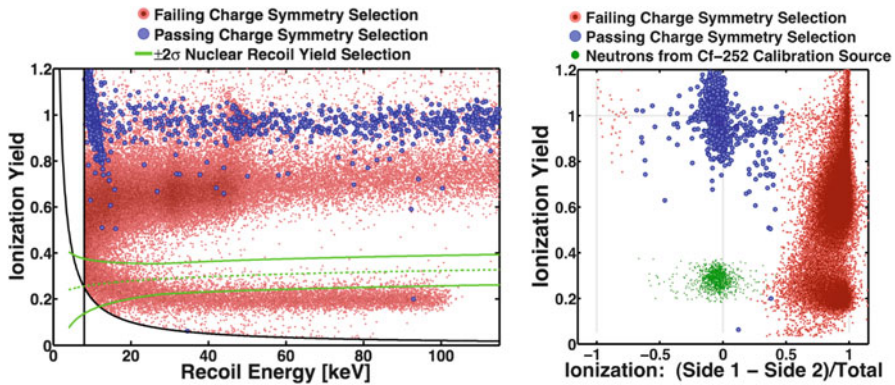


**Fig. 15.4** *Left*: Ionization yield versus phonon recoil energy for the same data, with  $2\sigma$  ionization yield selection of neutrons indicated (area within *green lines*). The *curving black line* is the ionization threshold (2 keV) and the *vertical black line* is the recoil energy threshold ( $8 \text{ keV}_{nr}$ ). Electrons from  $^{210}\text{Bi}$  (*red dots* at moderate ionization yield extending above 60 keV),  $^{210}\text{Pb}$  (*red dots* at moderate ionization yield below 60 keV), and  $^{206}\text{Pb}$  recoils (*red dots* at low ionization yield below  $\sim 100$  keV) are distinctly separated. *Right*: Nuclear recoils from  $^{252}\text{Cf}$  (*green*, low yield) and bulk electron recoils (*blue*, high yield) have symmetric ionization response between the side 1 and side 2 of the iZIP. Surface events from the  $^{210}\text{Pb}$  source (*red*), which is installed on side 1 of the detector, have an asymmetric response. Gammas and neutrons (*blue* and *green markers*) have a symmetric response. Outer radius events have been removed using the measured response on the guard electrode (Color figure online)

Combining the total phonon signal, charge signal, and charge asymmetry allows an impressive rejection of surface events, which were the dominant background of the previous CDMS II experiment. To measure the rejection capability of these new detectors, two of the detectors in SuperCDMS Sudan are exposed to a  $^{210}\text{Pb}$  source that emits about one electron per minute. Alpha particles and  $^{206}\text{Pb}$  nuclei are also ejected from the source and land on the detectors. Figure 15.4 shows the ionization yield on the y-axis, which is the ratio of ionization to phonon signals and is normalized to 1 for electron recoils. Figure 15.4 (left) shows phonon energy on the x-axis. In this plane, bulk electron recoils (blue) form a band around a yield of 1, while nuclear recoils lie in the green band around a yield of 0.3. All the red points are from the  $^{210}\text{Pb}$  source. The band around a yield of 0.7 and extending downwards is from the surface beta events. The band around a yield of 0.2 is from  $^{206}\text{Pb}$  nuclei impinging on the detector. One can clearly see the  $^{206}\text{Pb}$  endpoint at 103 keV, serving as an independent check on the nuclear energy scale calibration.

Figure 15.4 (right) shows the same data (except for nuclear recoils, which are shown in green events instead of a band) in the yield vs. charge symmetry plane. The events near zero on the x-axis had the same ionization signal on both sides; these symmetric events are thus generated in the bulk of the crystal. Events near  $\pm 1$  happened at one of the two surfaces. The red events from the  $^{210}\text{Pb}$  source divide into two populations, the betas at higher yield and the  $^{206}\text{Pb}$  events at lower yield.

Since the actual rate of  $^{206}\text{Pb}$  expected in the SNOLAB experiment is extremely small, we concentrate on the beta population. Out of 79,059 beta events, zero leak into the nuclear recoil region defined by these two plots. For an analysis threshold of 8 keV, in the absence of any measured leakage, a conservative upper bound is placed on the beta leakage of  $<2.9 \times 10^{-5}$  leakage events at the 90 % confidence level. This is not the final analysis of this data set, and as cuts are improved and more data is taken, a lower final limit is expected. With expected surface event rates of around 50 events/kg/year, this result already demonstrates detectors capable of several hundred kg-year exposure before running into leakage from surface events.

## 15.3 Conclusions

The SuperCDMS Soudan experiment is taking data and first science results are expected in 2013. This experiment will be sensitive to the region recently explored by XENON100, and will cover new parameter space in the low-mass region. Results from the new iZIP detectors at Soudan show impressive discrimination of surface events, paving the way for the SuperCDMS SNOLAB experiment, which if approved will begin construction in 2014.

## References

1. Komatsu, E., Dunkley, J., Nolte, M.R., Bennett, C.L., Gold, B., Hinshaw, G., Jarosik, N., Larson, D., Limon, M., Page, L., Spergel, D.N., Halpern, M., Hill, R.S., Kogut, A., Meyer, S.S., Tucker, G.S., Weiland, J.L., Wollack, E., Wright, E.L.: Seven-year Wilkinson Microwave Anisotropy Probe (WMAP) observations: cosmological interpretation. *Astrophys. J. Suppl. Ser.* **192**, 1–47 (2011)
2. Ahmed, Z., Akerib, D.S., Arrenberg, S., Bailey, C.N., Balakishiyeva, D., Baudis, L., Bauer, D.A., Brink, P.L., Bruch, T., Bunker, R., Cabrera, B., Caldwell, D.O., Cooley, J., do Couto e Silva, E., Cushman, P., Daal, M., DeJongh, F., Di Stefano, P., Dragowsky, M.R., Duong, L., Fallows, S., Figueroa-Feliciano, E., Filippini, J., Fox, J., Fritts, M., Golwala, S.R., Hall, J., Hennings-Yeomans, R., Hertel, S.A., Holmgren, D., Hsu, L., Huber, M.E., Kamaev, O., Kiveni, M., Kos, M., Leman, S.W., Liu, S., Mahapatra, R., Mandic, V., McCarthy, K.A., Mirabolfathi, N., Moore, D., Nelson, H., Ogburn, R.W., Phipps, A., Pyle, M., Qiu, X., Ramberg, E., Rau, W., Reisetter, A., Resch, R., Saab, T., Sadoulet, B., Sander, J., Schnee, R.W., Seitz, D.N., Serfass, B., Sundqvist, K.M., Tarka, M., Wikus, P., Yellin, S., Yoo, J., Young, B.A., Zhang, J.: Results from a low-energy analysis of the CDMS II Germanium data. *Phys. Rev. Lett.* **106**, 131302 (2011)
3. Ahmed, Z., Akerib, D.S., Arrenberg, S., Bailey, C.N., Balakishiyeva, D., Baudis, L., Bauer, D.A., Brink, P.L., Bruch, T., Bunker, R., Cabrera, B., Caldwell, D.O., Cooley, J., Cushman, P., Daal, M., DeJongh, F., Dragowsky, M.R., Duong, L., Fallows, S., Figueroa-Feliciano, E., Filippini, J., Fritts, M., Golwala, S.R., Grant, D.R., Hall, J., Hennings-Yeomans, R., Hertel, S.A., Holmgren, D., Hsu, L., Huber, M.E., Kamaev, O., Kiveni, M., Kos, M., Leman, S.W., Mahapatra, R., Mandic, V., McCarthy, K.A., Mirabolfathi, N., Moore, D., Nelson, H., Ogburn, R.W., Phipps, A., Pyle, M., Qiu, X., Ramberg, E., Rau, W., Reisetter, A., Saab, T., Sadoulet, B., Sander, J., Schnee, R.W., Seitz, D.N., Serfass, B., Sundqvist, K.M., Tarka, M., Wikus, P.,

- Yellin, S., Yoo, J., Young, B.A., Zhang, J.: Dark matter search results from the CDMS II experiment. *Science* **327**(5973), 1619–1621 (2010), [arXiv:0912.3592]
4. Armengaud, E., Augier, C., Benoit, A., Berge, L., Blumer, J., Broniatowski, A., Brudanin, V., Censier, B., Chardin, G., Chapellier, M., Charlieux, F., Coulter, P., Cox, G.A., Defayd, X., De Jesus, M., Dolgorouki, Y., Domange, J., Dumoulin, L., Eitel, K., Filosofov, D., Fourches, N., Gascon, J., Gerbier, G., Gironnet, J., Grosa, M., Henry, S., Herve, S., Juillard, A., Kluck, H., Kozlov, V., Kraus, H., Kudryavtsev, V.A., Loaiza, P., Marnieros, S., Navick, X.F., Nones, C., Olivieri, E., Pari, P., Pattavina, L., Paul, B., Robinson, M., Rozov, S., Sanglard, V., Schmidt, B., Scorza, S., Semikh, S., Torrento-Coello, A.S., Vagneron, L., Verdier, M.A., Walker, R.J., Yakushev, E.: Final results of the EDELWEISS-II WIMP search using a 4-kg array of cryogenic germanium detectors with interleaved electrodes. *Phys. Lett. B* **702**, 329–335 (2011), [arXiv:1103.4070]
  5. Ahmed, Z., Akerib, D.S., Armengaud, E., Arrenberg, S., Augier, C., Bailey, C.N., Balakishiyeva, D., Baudis, L., Bauer, D.A., Benoit, A., Berge, L., Blumer, J., Brink, P.L., Broniatowski, A., Bruch, T., Brudanin, V., Bunker, R., Cabrera, B., Caldwell, D.O., Censier, B., Chapellier, M., Chardin, G., Charlieux, F., Cooley, J., Coulter, P., Cox, G.A., Cushman, P., Daal, M., Defay, X., De Jesus, M., DeJongh, F., Di Stefano, P.C.F., Dolgorouki, Y., Domange, J., Dumoulin, L., Dragowsky, M.R., Eitel, K., Fallows, S., Figueroa-Feliciano, E., Filippini, J., Filosofov, D., Fourches, N., Fox, J., Fritts, M., Gascon, J., Gerbier, G., Gironnet, J., Golwala, S.R., Gros, M., Hall, J., Hennings-Yeomans, R., Henry, S., Hertel, S.A., Herve, S., Holmgren, D., Hsu, L., Huber, M.E., Juillard, A., Kamaev, O., Kiveni, M., Kluck, H., Kos, M., Kozlov, V., Kraus, H., Kudryavtsev, V.A., Leman, S.W., Liu, S., Loaiza, P., Mahapatra, R., Mandic, V., Marnieros, S., Martinez, C., McCarthy, K.A., Mirabolfathi, N., Moore, D., Nadeau, P., Navick, X.-F., Nelson, H., Nones, C., Ogburn, R.W., Olivieri, E., Pari, P., Pattavina, L., Paul, B., Phipps, A., Pyle, M., Qiu, X., Rau, W., Reisetter, A., Ricci, Y., Robinson, M., Rozov, S., Saab, T., Sadoulet, B., Sander, J., Sanglard, V., Schmidt, B., Schnee, R.W., Scorza, S., Seitz, D.N., Semikh, S., Serfass, B., Sundqvist, K.M., Tarka, M., Torrento-Coello, A.S., Vagneron, L., Verdier, M.-A., Walker, R.J., Wikus, P., Yakushev, E., Yellin, S., Yoo, J., Young, B.A., Zhang, J.: Combined limits on WIMPs from the CDMS and EDELWEISS experiments. *Phys. Rev.* **D84**, 011102 (2011)
  6. Aprile, E., Arisaka, K., Arneodo, F., Askin, A., Baudis, L., Behrens, A., Bokeloh, K., Brown, E., Bruch, T., Bruno, G., Cardoso, J.M.R., Chen, W.-T., Choi, B., Cline, D., Duchovni, E., Fattori, S., Ferella, A.D., Gao, F., Giboni, K.-L., Gross, E., Kish, A., Lam, C.W., Lamblin, J., Lang, R.F., Levy, C., Lim, K.E., Lin, Q., Lindemann, S., Lindner, M., Lopes, J.A.M., Lung, K., Marroddan Undagoitia, T., Mei, Y., Melgarejo Fernandez, A.J., Ni, K., Oberlack, U., Orrigo, S.E.A., Pantic, E., Persiani, R., Plante, G., Ribeiro, A.C.C., Santorelli, R., dos Santos, J.M.F., Sartorelli, G., Schumann, M., Selvi, M., Shagin, P., Simgen, H., Teymourian, A., Thers, D., Vitells, O., Wang, H., Weber, M., Weinheimer, C.: Dark matter results from 100 live days of XENON100 data, [arXiv:1104.2549v2]
  7. Angloher, G., Bauer, M., Bavykina, I., Bento, A., Bucci, C., Ciemniak, C., Deuter, G., von Feilitzsch, F., Hauff, D., Huff, P., Isaila, C., Jochum, J., Kiefer, M., Kimmerle, M., Lanfranchi, J.-C., Petricca, F., Pfister, S., Potzel, W., Probst, F., Reindl, F., Roth, S., Rottler, K., Sailer, C., Schaffner, K., Schmalzer, J., Scholl, S., Seidel, W., von Sivers, M., Stodolsky, L., Strandhagen, C., Straus, R., Tanzke, A., Usherov, I., Wawoczny, S., Willers, M., Zoller, A.: Results from 730 kg days of the CRESST-II dark matter search, [arXiv:1109.0702]
  8. Hooper, D., Collar, J.I., Hall, J., McKinsey, D., Kelso, C.M.: Consistent dark matter interpretation for CoGeNT and DAMA/LIBRA. *Phys. Rev. D* **82**, 123509 (2010)
  9. Strece, C., Bertone, G., Cerdeno, D.G., Fornasa, M., Ruiz de Austri, R., Trotta, R.: Updated global fits of the cMSSM including the latest LHC SUSY and Higgs searches and XENON100 data. *J. Cosmol. Astropart. Phys.* **03**, 030 (2012), [arXiv:1112.4192]